



TECHNICAL ARTICLE

Variation in Centrifugal Speed and Resultant Changes in Microstructure and Properties of ZrO₂-Toughened Al₂O₃ Particle-Reinforced Iron Matrix Composites

Zhijie Wang, Ge Niu, Yudong Sui, Yehua Jiang, and Mojin Zhou

Submitted: 2 June 2022 / Revised: 3 October 2022 / Accepted: 5 October 2022 / Published online: 31 October 2022

Honeycomb-structured high-chromium cast iron (HCCI) composites reinforced with ZrO₂-toughened Al₂O₃ (ZTA) particles were prepared through centrifugal casting. Centrifugal speeds had a significant impact on the microstructure and the performance of the composites during the centrifugal casting process. As the centrifugal speeds (600, 700, 800, 900 r/min) increased, the austenitic microstructure and eutectic carbides of the composites were obviously refined as a result of nucleation area increase caused by dendrite fragmentation. Meanwhile, with a change in centrifugal speed, the hardness of the composites increased by 5 HRC. The results of three-body abrasive wear under high-stress load showed that the wear volume loss of the composites decreased with the centrifugal speeds. The wear resistance of the composites at 900 r/min was 1.45 times higher than that at 600 r/min. A reasonable centrifugal speed, therefore, is recommended in this study to prepare the ZTA/HCCI composites with better microstructure and mechanical properties.

Keywords centrifugal casting, high-chromium cast iron, iron matrix composite, three-body abrasive wear resistance, ZrO₂-toughened Al₂O₃

1. Introduction

With good thermal stability, better fracture toughness, and thermal expansion coefficient closer to the iron matrix, ZTA ceramic particles are considered as the most suitable material for reinforcing iron matrix composites (Ref 1, 2). Iron matrix composites with ZTA particles are used in many fields, including mineral processing and industrial applications because of their mature preparation technology, relatively low cost, and good wear resistance (Ref 3-5). When making rotary parts such as grinding rollers with ceramic particles on the external surface, traditional gravity casting technology encounters some difficulties (Ref 6, 7). Currently, centrifugal casting is mostly used in the preparation of partially reinforced rotary parts, which enjoys better filling performance, denser microstructure, finer carbides, and a simple casting process (Ref 8-10). During centrifugal casting, the centrifugal speeds have a great influence on the microstructure and properties of the composites. The effect of mold rotation speeds on the gradient microstructure and properties of WC/Fe-C composites

was investigated by Song et al. (Ref 11). The results showed that the hardness and impact toughness of the working layer in the composites changed with the increase in the mold rotation speed. Yang et al. (Ref 12) studied the effect of centrifugal casting speeds on the forming pattern of castings. It was found that the increase in centrifugal speeds could bring finer micro grains and higher hardness. Niu et al. (Ref 13) studied in situ particle-reinforced iron matrix composites prepared by using centrifugal casting. The results showed that the composites containing a high volume fraction of hard WC had higher wear resistance than gray cast iron without any enforcement.

Centrifugal speeds can significantly affect the movement of particles, with inappropriate speeds leading uneven particle distribution and casting defects (Ref 14). But only a few reports on the relationship between centrifugal casting speeds and the microstructure and wear resistance of high-chromium cast iron (HCCI) matrix composites reinforced with ZTA particles have been conducted. This paper, therefore, focuses on the effect of centrifugal speeds on the microstructure, mechanical properties, and wear resistance in ZTA/HCCI composites prepared by using centrifugal casting.

2. Experimental Procedure

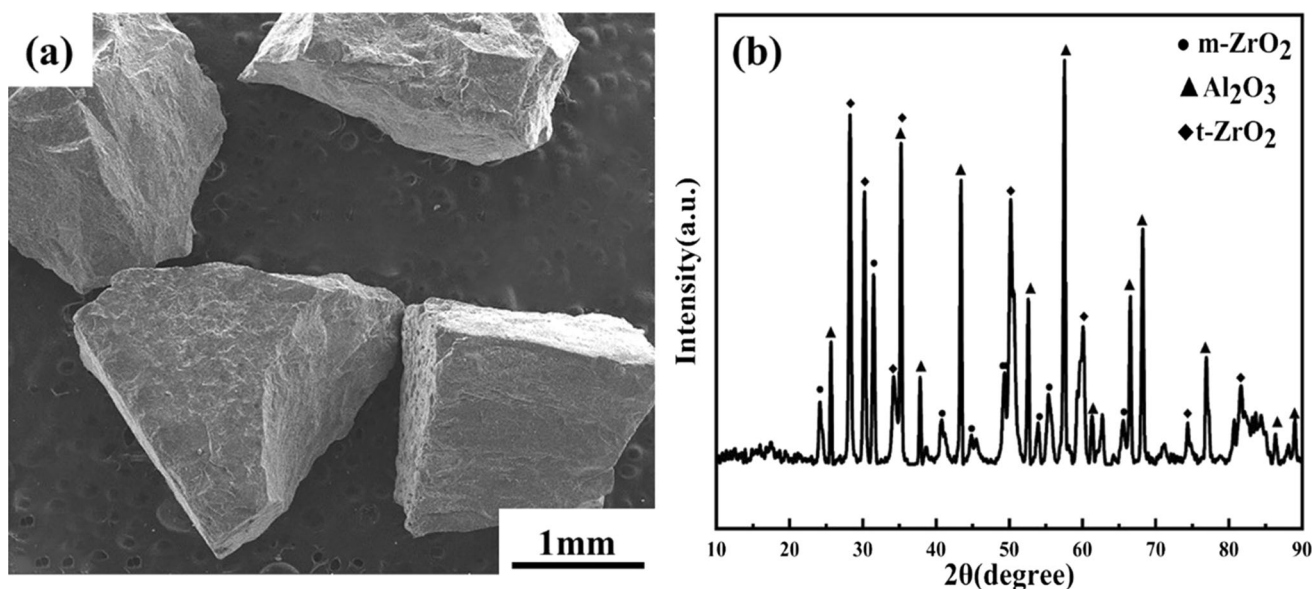
2.1 Materials

In this study, HCCI was selected as the matrix, and its chemical composition is presented in Table 1. ZTA particles with a 2 mm diameter were selected as the reinforcement material, and they consisted of 56% Al₂O₃, 40% ZrO₂, 3% TiO₂, and 1% Fe₂O₃ (wt.%). They had 1500-1600 HV in microhardness, 4.3 g·cm⁻³ in density, 1890 °C in melting point, and 8.5 × 10⁻⁶/°C in thermal expansion coefficient. The SEM micrograph and x-ray diffraction results of the ZTA particles are shown in Fig. 1.

Zhijie Wang, Ge Niu, Yudong Sui, and Mojin Zhou, School of Materials Science and Engineering, Kunming University of Science and Technology, Kunming 650093, People's Republic of China; **Yehua Jiang**, National & Local Joint Engineering Laboratory of Advanced Metal Solidification Forming and Equipment Technology, Kunming University of Science and Technology, Kunming 650093, People's Republic of China. Contact e-mails: jiangyehua@kmust.edu.cn and zhoumojin@kmust.edu.cn.

Table 1 Chemical composition of high-chromium white cast iron matrix (wt.%)

Element	C	Si	Cr	Mn	S	P	Mo	Ni	Fe
Content, wt.%	2.5-2.9	0.4-0.6	19-22	0.7-0.8	≤ 0.01	≤ 0.04	0.3-0.5	0.3-0.5	Bal.

**Fig. 1** (a) SEM micrograph and (b) x-ray diffraction result of ZTA particles

2.2 Composites Preparation

The HCCI composites refined with ZTA particles were prepared by using centrifugal casting. The J-517 horizontal centrifugal casting machine used is produced by Jinan Haomai Casting Machinery Co., Ltd., and the casting process is shown in Fig. 2. To obtain the preforms for the experiment, the ZTA particles were coated with ceramic powder to improve the wettability of the HCCI matrix, and then, they were mixed with Na_2SiO_3 solution to make the bonding agent fixed in the mold. The preforms have 120 mm inner diameter, 30 mm thickness, and 300 mm height, and its honeycomb structure is shaped like a regular hexagon with a 10 mm wall thickness and 12.5 mm hole diameter. In the first step, the preforms were fixed in the inner cavity of the mold and preheated to 150 ~ 250 °C. Then, a melting furnace with medium frequency was used to melt the HCCI melt with a pouring temperature of 1600 °C, and four different sets of parameters (600 r/min, 700 r/min, 800 r/min, and 900 r/min) were used in the empirical formula of gravity centrifugation: $n = 299 \sqrt{\frac{G}{R}}$ (G: gravity coefficient, cast iron = 30 ~ 70) (Ref 15). This was gained from the equation (Ref 16, 17). $G = \frac{\omega^2 R}{g} = \frac{N^2 \pi^2}{900g} R$ (G, ω , N, R, and g represent gravity coefficient, angular velocity (rad/s), the rotating speed of the centrifugal (r/min), the distance from the centrifugal axis to the center of sample (m), and normal-gravitational acceleration, respectively.) In the last step, the melt was cooled to room temperature, and the honeycomb-structured iron matrix composites refined with ZTA particles were made.

2.3 Three-Body Abrasive Wear Test

Three-body abrasive wear tests were conducted on an MFG-800SQ abrasive wear tester produced by Jinan Siernuo Machinery Equipment Co., LTD. Each wear sample was 30 × 20 × 20 mm with a 45° angle and was fixed by clamps. The wear direction in the experiment was parallel to that of the wear surface of the sample. Silica sands with a size of 0.6 mm were used as the abrasive. The load was 600 N and the speed was 1500 mm/min. In addition, to ensure accuracy, the abrasive particles were replaced every one hour. The sample was pre-worn for 1 h before experiencing 12 grinding processes, each of which lasted for 1 h. The remaining other steps and the method used to calculate the volume loss of the composite were the same as those in these two papers (Ref 18, 19).

2.4 Characterization

The surfaces of the sample were polished and etched in nitrates with 4 vol.% alcohol to reveal their microstructure. The microstructure and wear morphology of the composites were observed through a metallographic microscope (Nikon-M300), scanning electron microscope (SEM, ZEISS-EVO18), and energy-disperse spectroscopy (EDS). The phase composition of the sample was identified through x-ray diffraction (XRD, D/max-2500). The overall mechanical properties of the ZTA/HCCI composites were tested in a compression tester (SHT-4305), and the compression samples were 15 × 15 × 25 mm

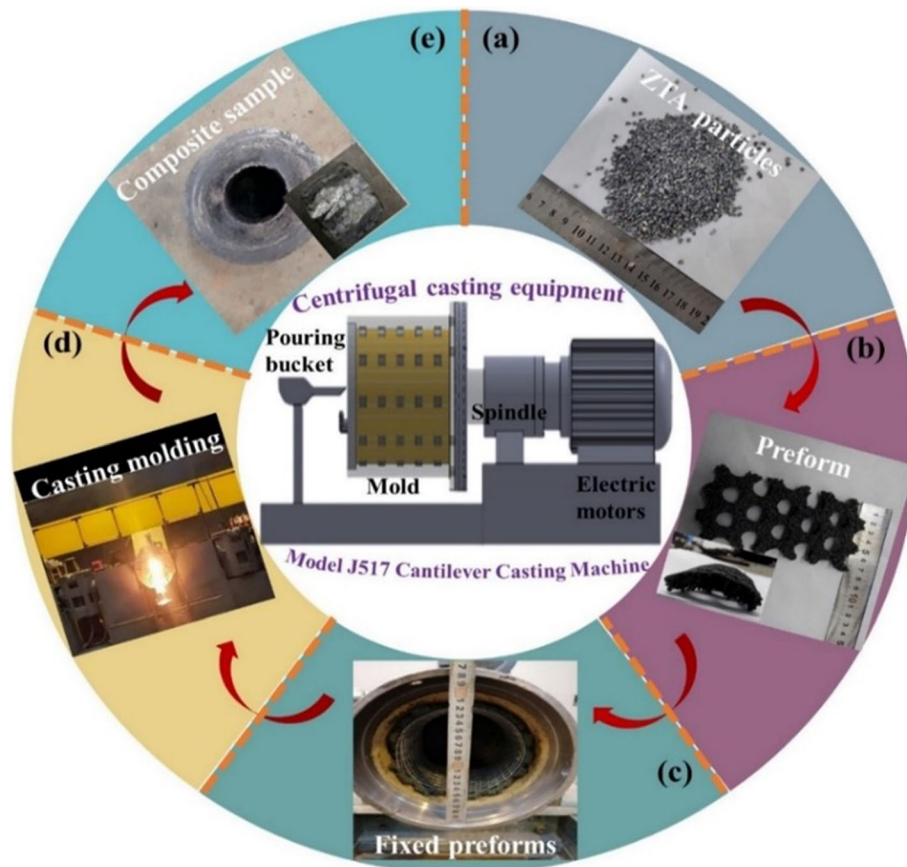


Fig. 2 Flowchart of ZTA/HCCI composite prepared by using centrifugal casting: (a) ZTA image; (b) preparation of preforms; (c) fixed preforms; (d) casting process; (e) composites sample

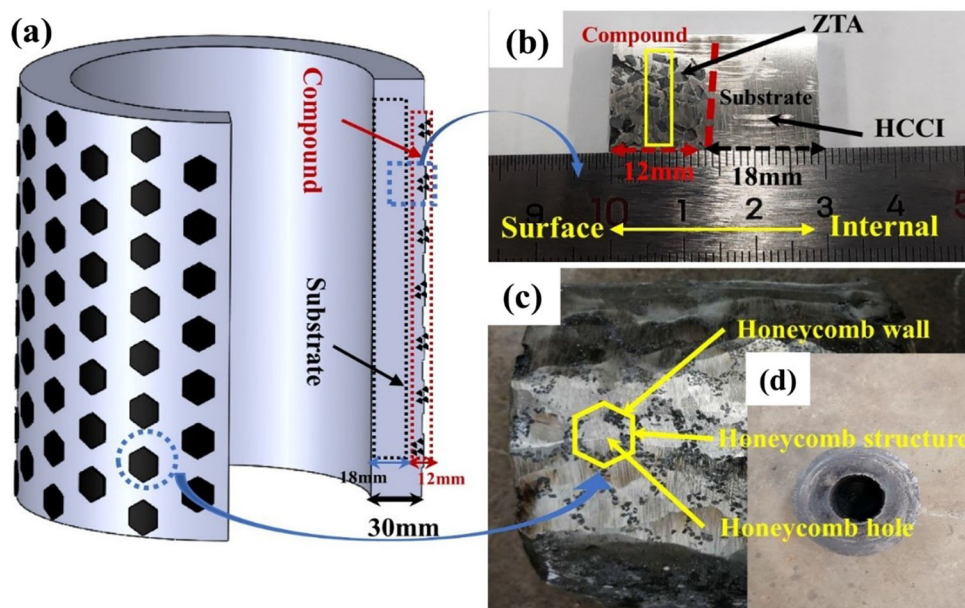


Fig. 3 Surface and cross section morphology view of the rotating parts in the composites: (a) Schematic of the rotating parts, (b) local sample of the composites, (c) macroscopic morphology of composites surface, (d) top macroscopic morphology view of the composites

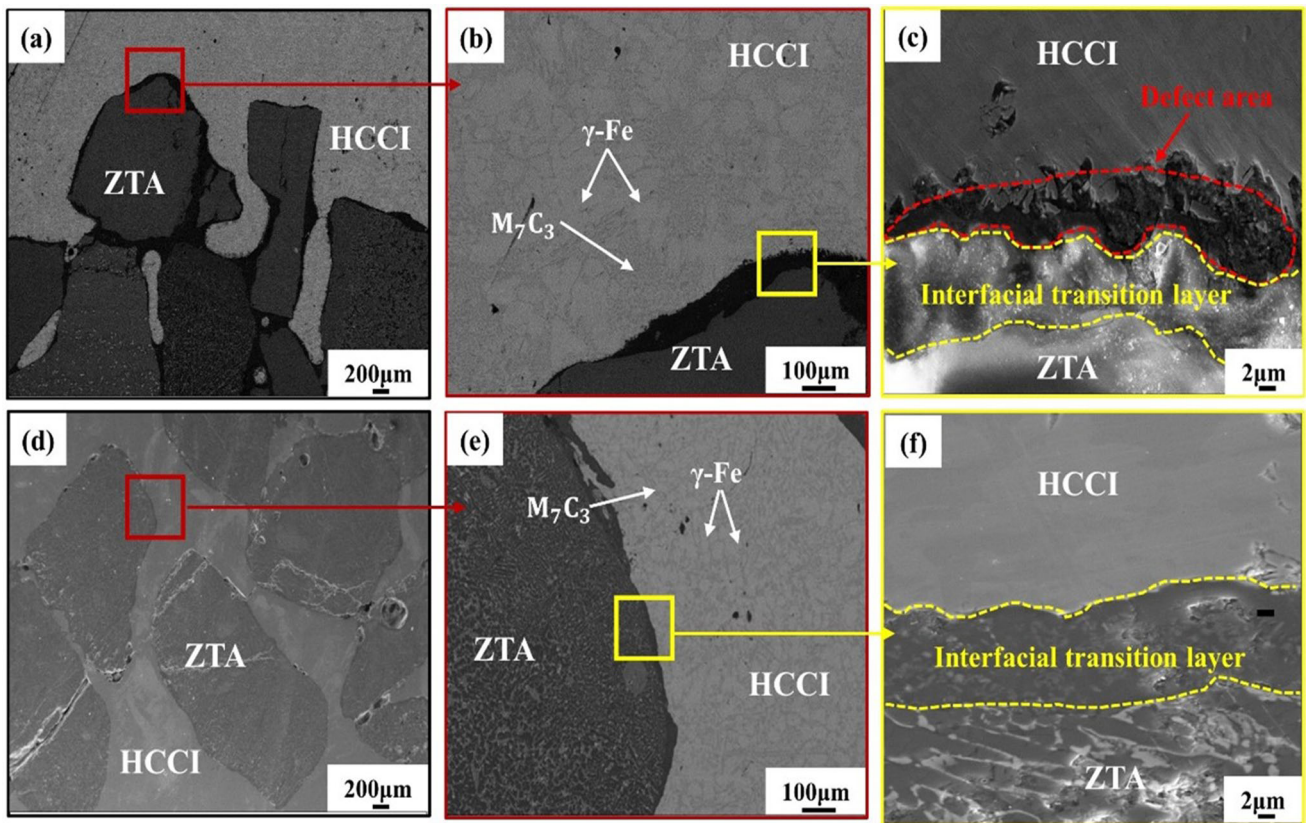


Fig. 4 Distribution of ZTA particles throughout the HCCI matrix, the microstructure and interface bonding microstructure of the composites at 600 r/min (a-c) and 900 r/min (d-f)

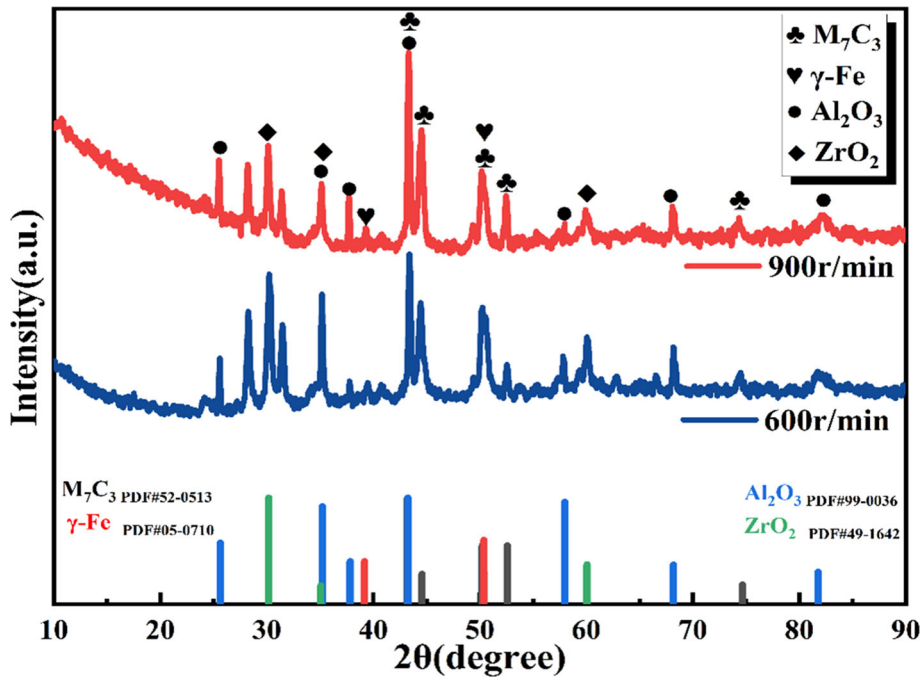


Fig. 5 X-ray diffraction analysis of composites at 600 r/min and 900 r/min

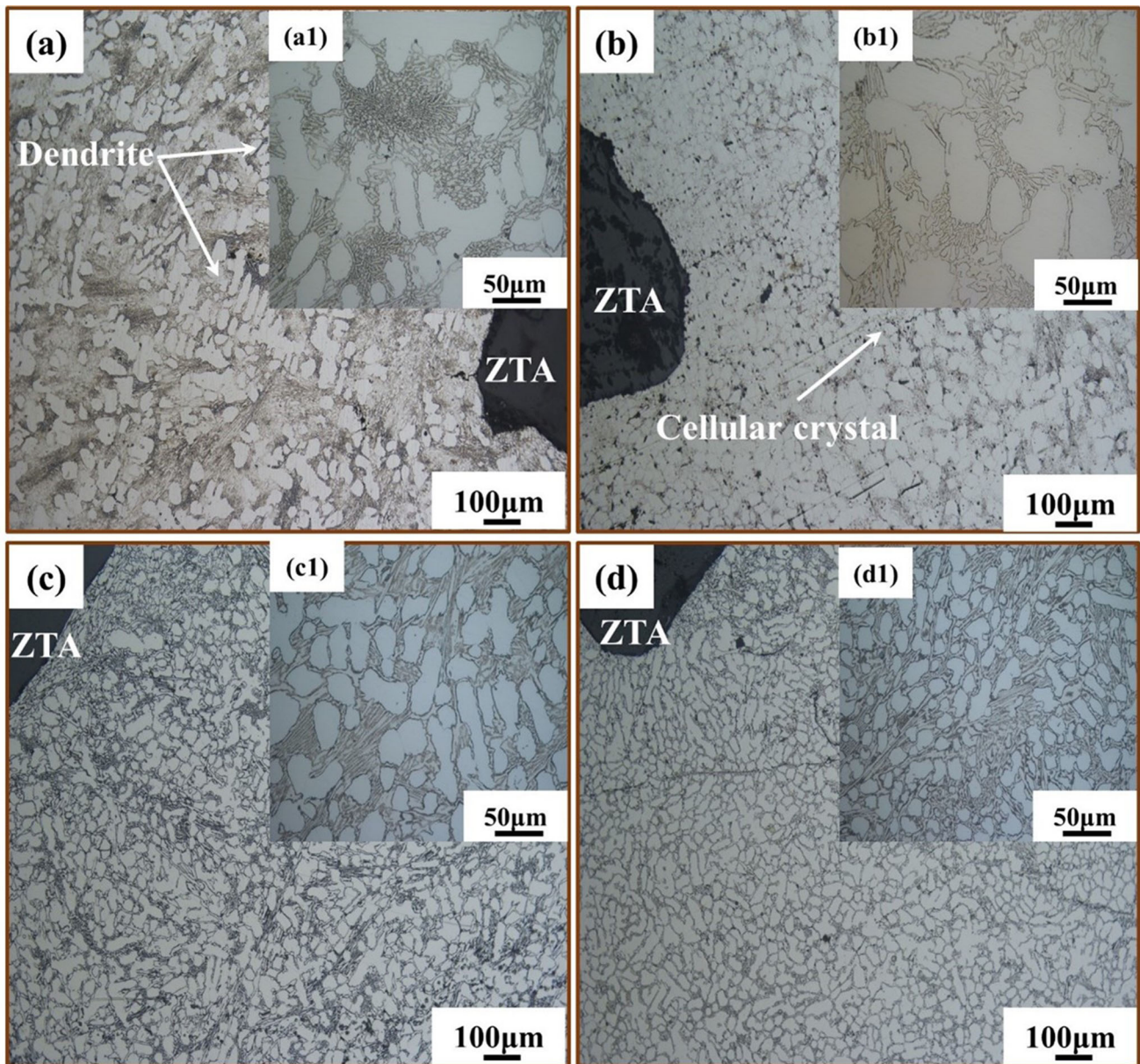


Fig. 6 Metallographic micrographs of the centrifugal casting composites at different casting speeds: (a) 600 r/min, (b) 700 r/min, (c) 800 r/min, (d) 900 r/min

in size and 0.5 mm/min in speed, which was based on the GB/T7314-2005 Chinese standard.

3. Results and Discussion

3.1 The Morphology Surface Microstructure of the Composites

Figure 3 shows the schematic and sectional view of the ZTA/HCCI composites prepared by using centrifugal casting. The composites are mainly composed of the HCCI matrix and ZTA/HCCI compound. The 12-mm-thick compound area is on the outer surface, and the matrix area is 18 mm thick. As can be seen from Fig. 3(b), the ZTA particles were uniformly distributed in HCCI, and no pores or significant inclusions were found in the interior of the rotary parts in the composites. In

addition, from Fig. 3(c), it can be observed that the surface layer of the composites had a honeycomb structure. The image can also prove the completeness of such a structure and the absence of obvious defects on the surface. The middle part of the composites was selected for the analysis of their microstructure and mechanical properties, as shown in the yellow box in Fig. 3(b).

The ZTA ceramic particles were distributed in the HCCI matrix, whose microstructure and the interfacial bonding of the composite are shown in Fig. 4. When the centrifugal speeds were at 600 r/min and 900 r/min, the distribution of the ZTA particles in the HCCI matrix was relatively uniform, and only a few particles gathering together, which might be caused by the uneven coating of the bonding agent during the preform preparation. As seen in Fig. 4(b), the austenite microstructure at 900 r/min was finer than that at 600 r/min, and the M_7C_3 -type carbides were distributed around it. In addition, it can be seen

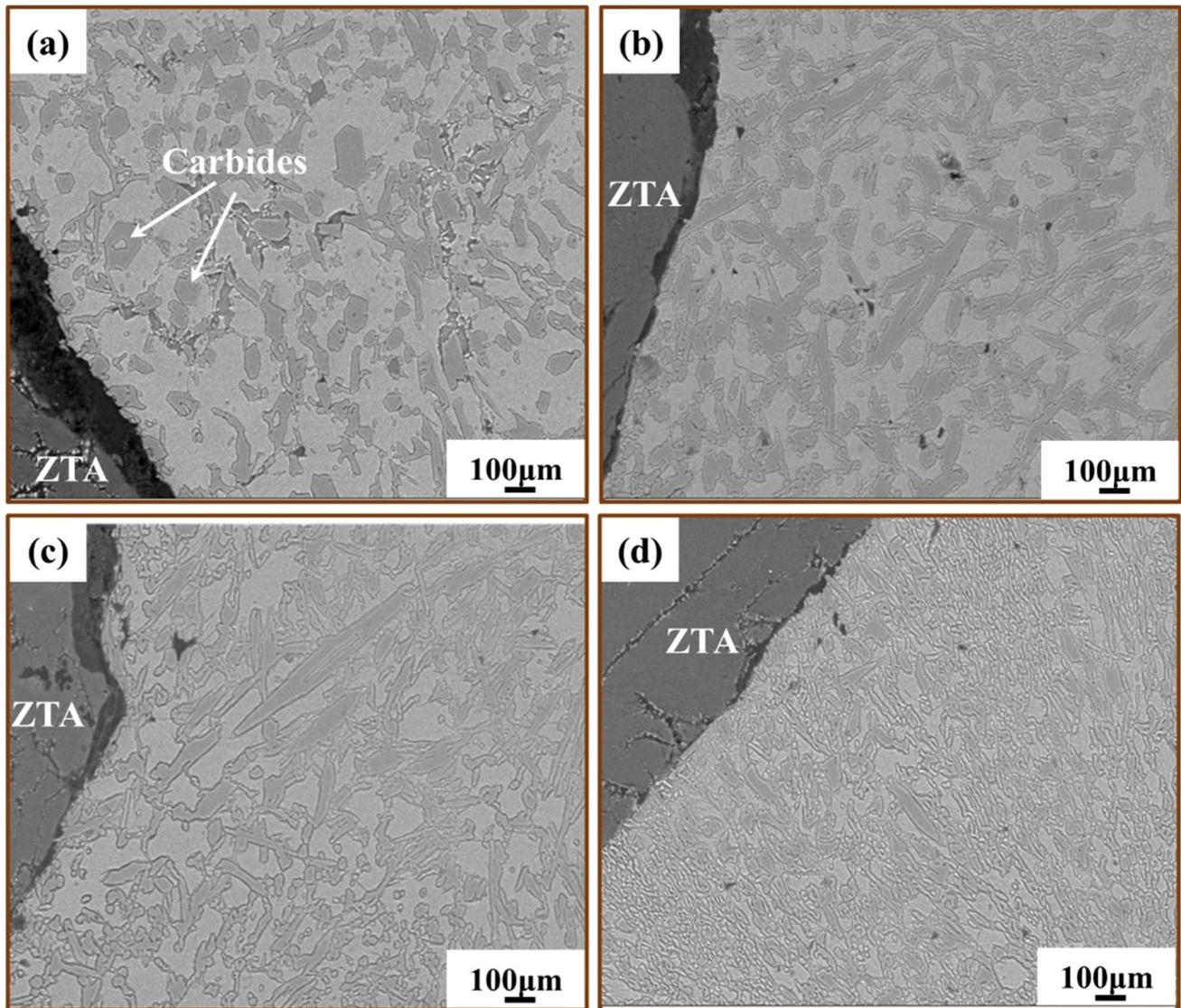


Fig. 7 SEM of carbide morphology of the centrifugally casting composites at different casting speeds: (a) 600 r/min, (b) 700 r/min, (c) 800 r/min, (d) 900 r/min

from Fig. 4(c) that at a speed of 600 r/min the interfacial transition layer had obvious defects, which were discontinuous and non-uniform, while at the speed of 900 r/min the centrifugal pressure increased due to the increase in the centrifugal speed. As the centrifugal pressure increases, the cast infiltration pressure will rise, which brings a better bonding effect and excellent interfacial transition layers between the ZTA particles and the HCCI matrix(Ref 20). The existence of good interfacial transition layers not only improves the interfacial bonding effect but also provides good stress relief, between the ZTA particles and the HCCI matrix, and brings transferring loads and other advantages, which improves the overall mechanical properties of the composites (Ref 21).

Analysis was made to determine the phase composition of the ZTA/HCCI composites by using XRD. From the x-ray diffraction results shown in Fig. 5, the phase composition was mainly austenite (γ -Fe), M_7C_3 carbides, Al_2O_3 , and ZrO_2 . This result is consistent with the microstructure shown in Fig. 4,

with the large white area in the HCCI matrix being the austenite, the gray part being M_7C_3 carbides, and the white ZrO_2 in the ZTA particles distributed in the Al_2O_3 . It was found that the change of centrifugal speeds alone did not cause the change of phase composition under the same other conditions for preparation. The phase composition of the ZTA/HCCI composites, therefore, is the same under different centrifugal speeds.

Figure 6 shows the microstructure of the composites at four centrifugal speeds, and it can be seen that with the increase in the centrifugal speeds, the microstructure was significantly refined, and the thick dendrites gradually became cellular crystals. The sizes of austenite grains at different speeds were compared by using Image-Pro Plus, as shown in Fig. 8(a), in which the austenite was reduced from 46 to 20 μm . This is because the increase in centrifugal speeds brought higher centrifugal force which increased the possibility of dendritic fracture that would lead to an increase in the number of

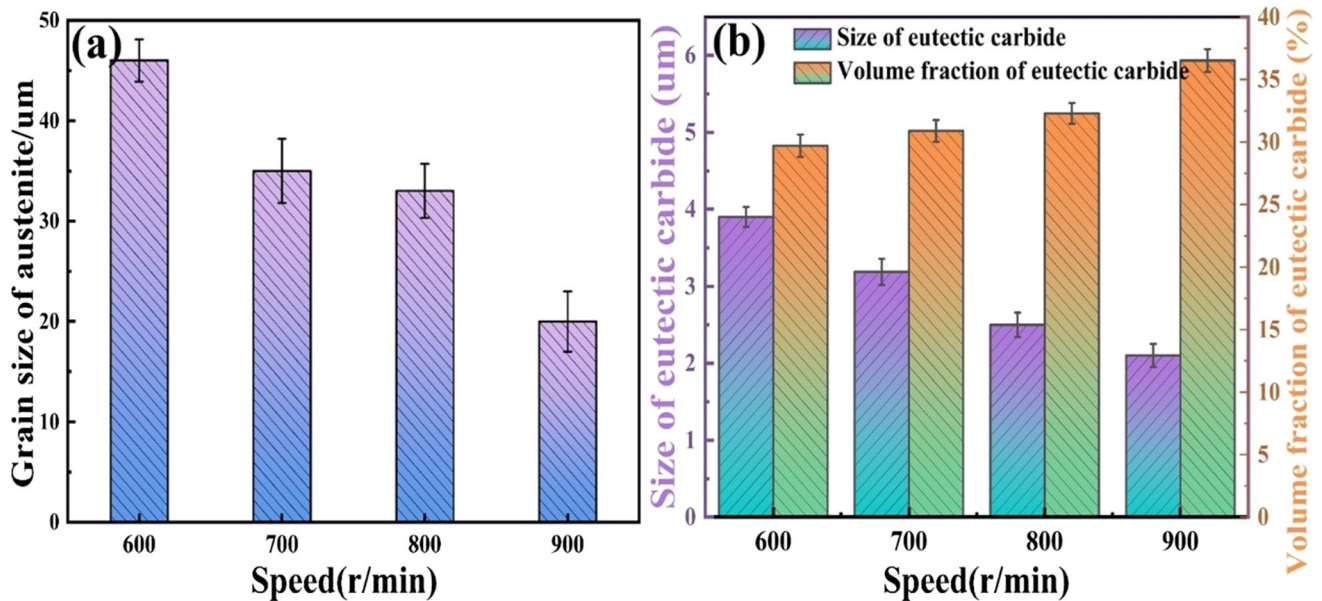


Fig. 8 (a) Grain size versus centrifugal speed for austenite of the composites, (b) Size and volume fraction of eutectic carbides of the composites at different centrifugal speeds

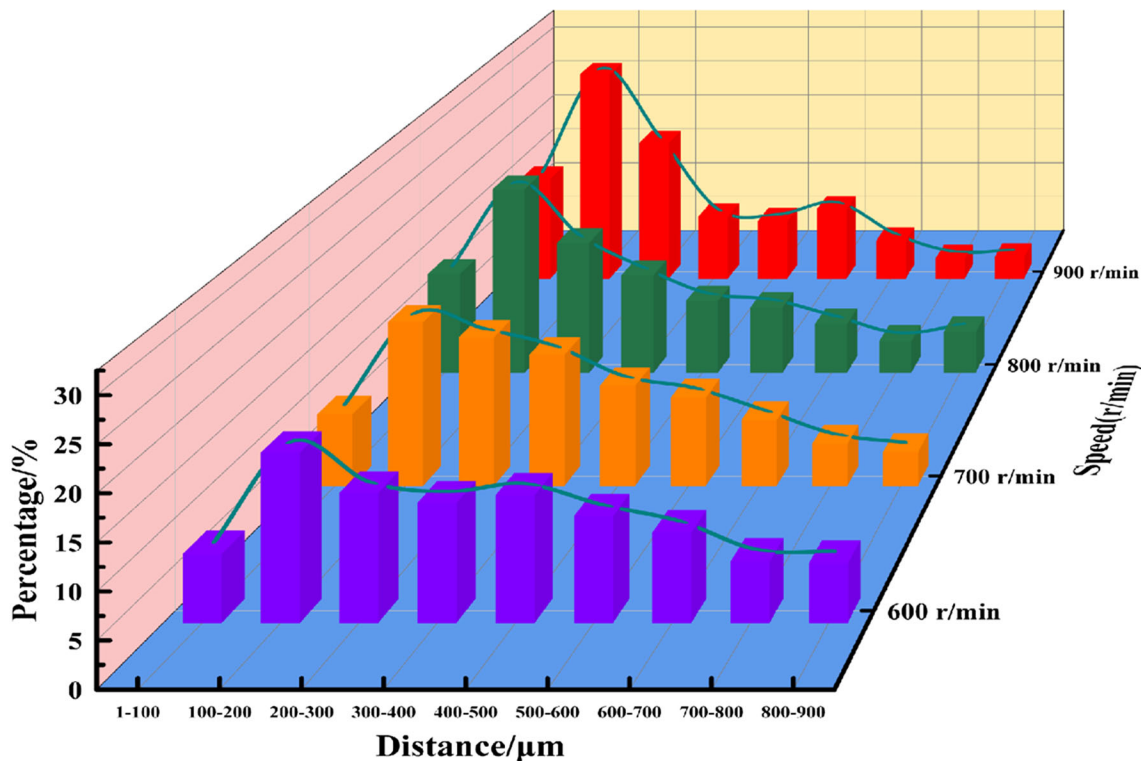


Fig. 9 Effect of different centrifugal speeds on the distribution spacing of ZTA particles

nucleation points, thus reducing the size of austenite grains (Ref 22). Meanwhile, the broken dendrites would be transformed into cellular crystals (Ref 23, 24). In addition, as the centrifugal speed went up, the movement of ZTA particles increased, and the austenite dendrites at the early stage of solidification collide with each other and became broken and refined (Ref 25, 26).

As can be seen in Fig. 7, the areas in dark gray are carbides, and the gray–white parts are austenite. Mostly, the morphology of carbides is hexagonal, dotted, C-shaped, and rod-shaped.

With the increase in the centrifugal speeds, the carbide morphology changed significantly. At 600 r/min, the carbides looked hexagonal, short-rod alike and coarse with different sizes, and had a strong cutting effect on the matrix. At 900 r/min, however, the coarse rod-like carbides became fine and diffuse. In addition, as can be seen from Fig. 8(b), as the centrifugal speed increased, the size of the carbide decreased from 3.9 to 2.1 μm , and their volume fraction rose from 29.7 to 36.5%. The change in the carbide morphology was due to the

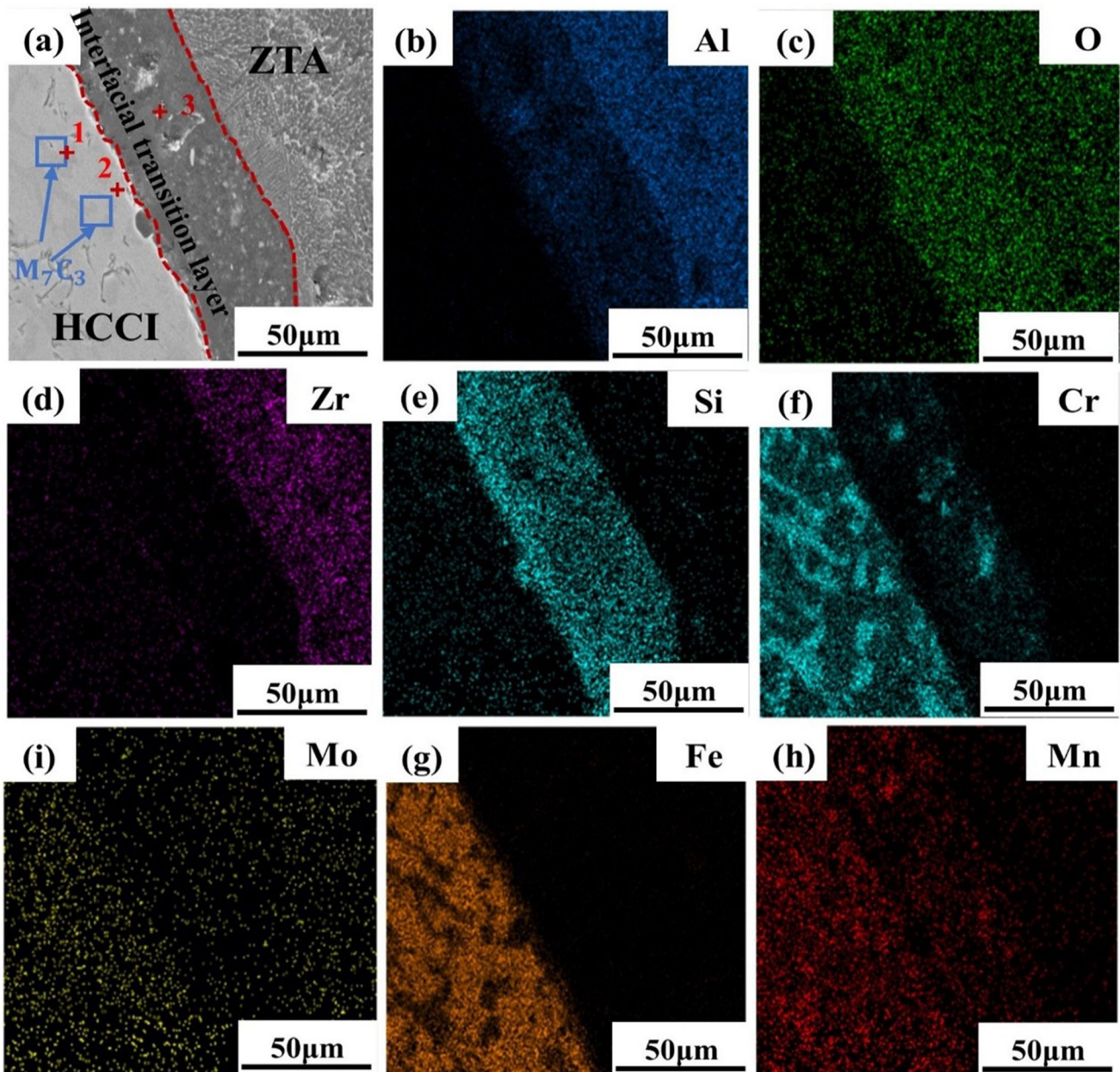


Fig. 10 EDS mapping of the ZTA/HCCI composite: (a) SEM image, (b-h) maps of different elements

Table 2 EDS analysis results for the point in Fig. 10 (at.%)

Point	Cr	Fe	Si	Al	O	Ni	Mo	Zr	Mn
1	57.2	40.2	0.4	0.6	0.8	0	0.2	2.08	0.6
2	15.7	78.2	4.1	0.3	0.8	0.3	0	0	0.6
3	1.5	0.3	14.8	19.7	63.0	0	0	0	0.8

possible destabilization of the solid–liquid solidification interface as a result of the centrifugal speed increase, which had some effect on its growth pattern (Ref 27). Meanwhile, as the centrifugal speed increased, it was easier for carbides to be nucleated because of the decrease in ZTA particle spacing and the increase in undercooling caused by tighter casting. This made the nucleation growth diffuse Fe, Cr, and C elements

slower, bringing fine and uniformly distributed carbides (Ref 28, 29). In addition, it was also related to the refinement of austenite. As generally carbides are in austenite dendrites during their growth, carbides could only be nucleated in the fine eutectic austenite when the coarse dendrites disappeared, which brought more areas for nucleation and smaller sizes of carbides (Ref 30).

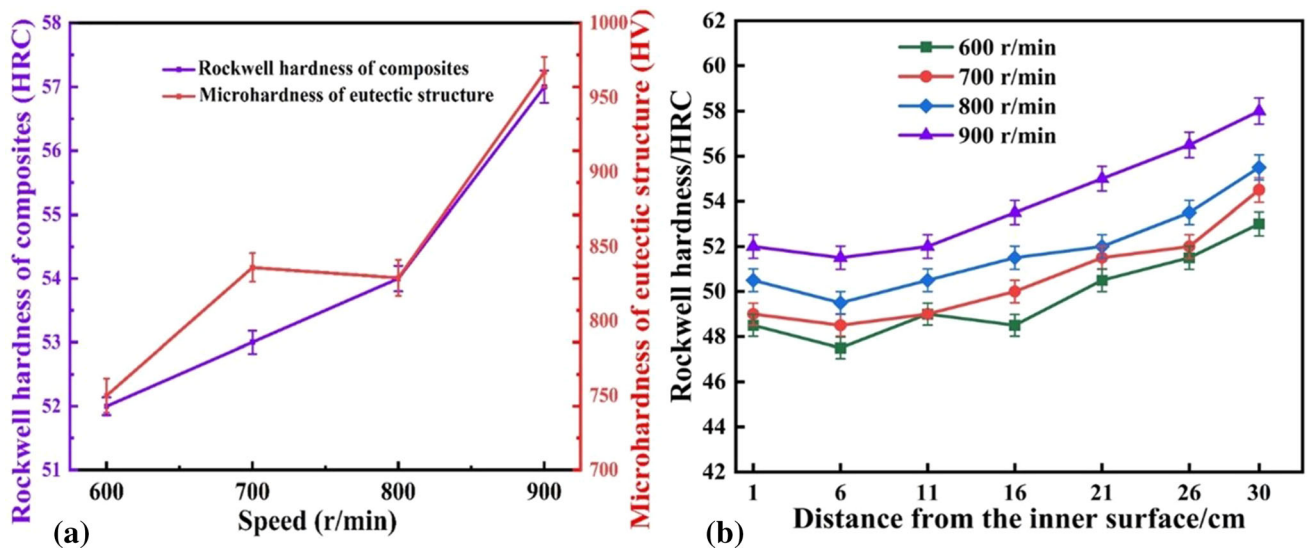


Fig. 11 (a) Effect of different speeds on hardness in the matrix and the centrifugal casting composites, (b) radial Rockwell hardness of the inner surface at different casting speeds

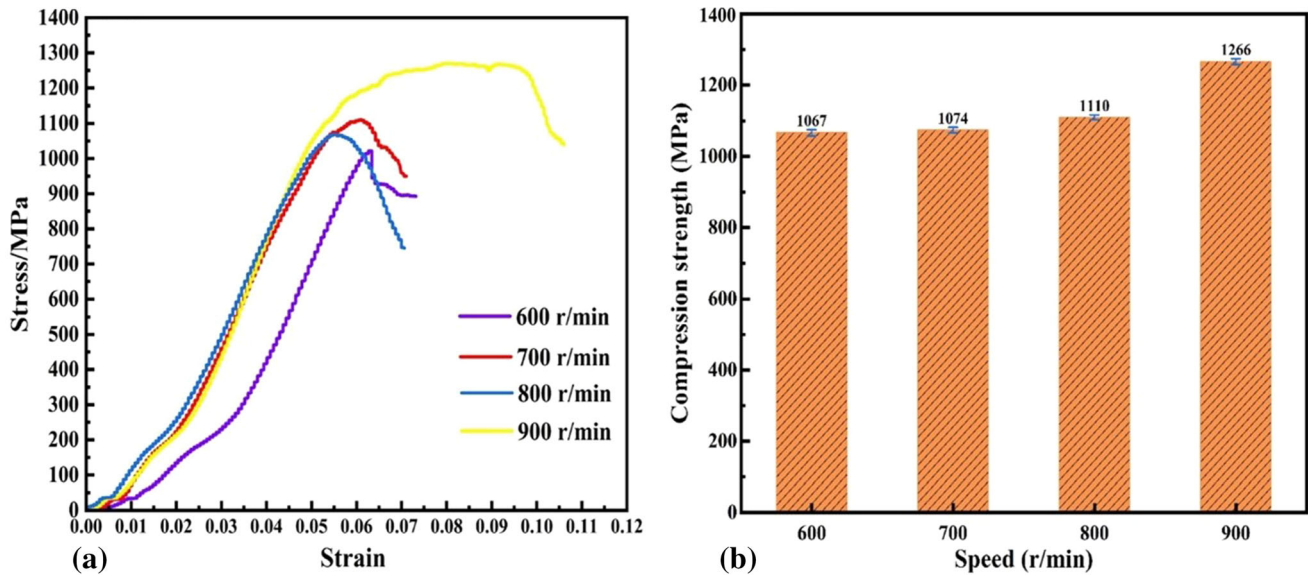


Fig. 12 (a) Stress–strain curves, (b) compression strength values

Changes in the centrifugal speeds had a great influence on the distribution of ZTA particles. As the centrifugal speeds rose, the increase in centrifugal force produced less dense ZTA particles moving toward the inner surface of the casting, as shown in Fig. 9. At 600 r/min, the ZTA particles moved slowly and the particles were dispersedly distributed before solidification. At 900 r/min, however, the ZTA particles moved faster, and they were closely distributed before solidification, and most of them were 100-300 μm in size. This phenomenon shows that centrifugal speed changes would bring an obvious gradient in terms of the distribution of ZTA particles. This was because as the centrifugal speed increased, the centrifugal force became bigger, making the ZTA particles gather faster toward the inner

surface of the casting under the centrifugal force, thus making the ZTA particles more closely distributed.

Figure 10 shows the morphology and elemental mapping results of EDS of the ZTA/HCCI composites. The transition layers between ZTA particles and the HCCI matrix are continuous, complete, and homogeneous, with good interfacial bonding ability between ZTA particles and the HCCI matrix. In Fig. 10(a), (f) (position 1), and Table 2 (points 1), the rectangle box represents the carbides, which maintained a tight contact with the HCCI matrix. It can be proved that it is the HCCI matrix from Fig. 10(a), (g) (position 2) and Table 2 (points 2). The HCCI matrix was found to be closely bonded with the transition layer. Position 3 in Fig. 10(a) is the transition layer

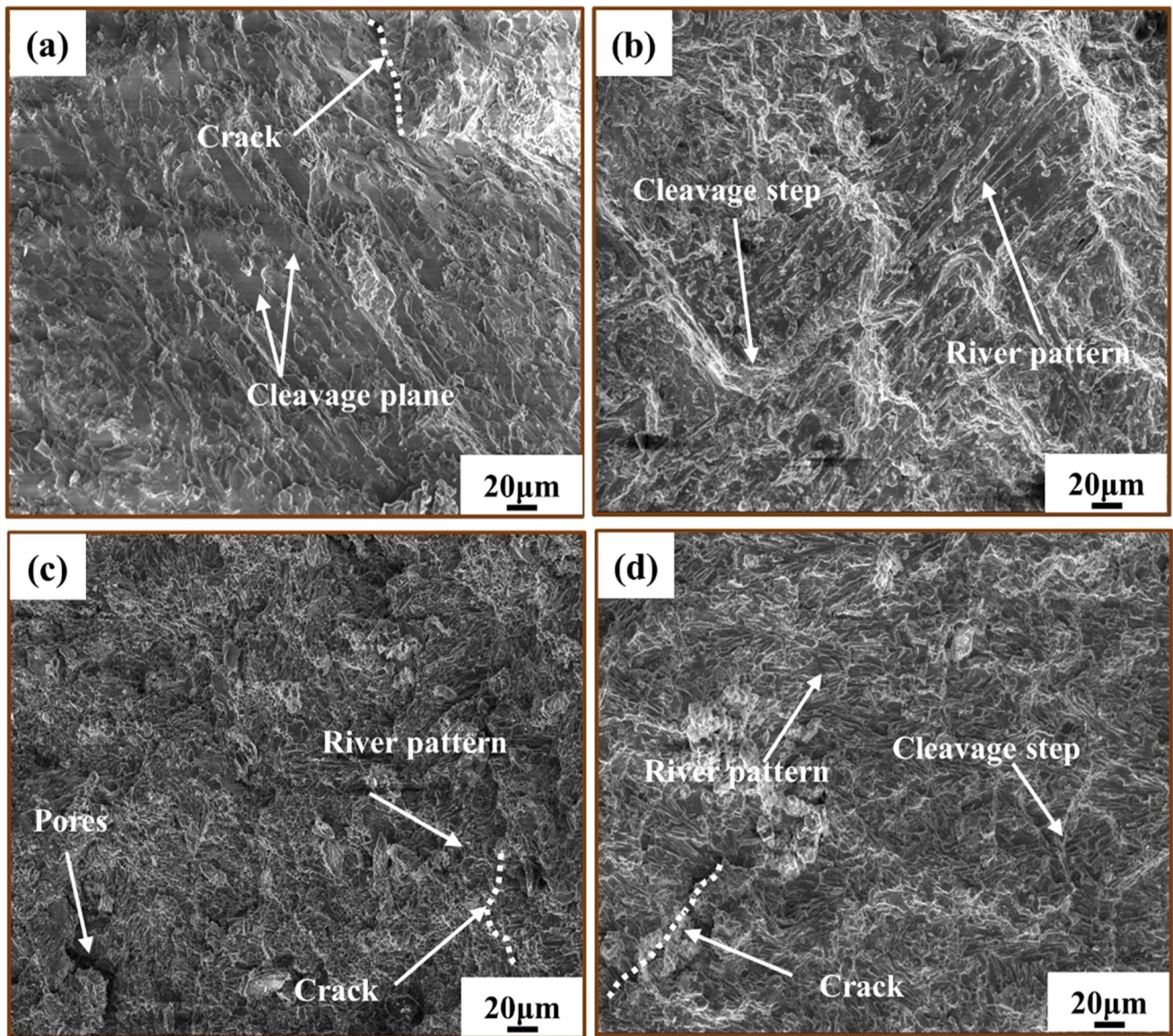


Fig. 13 Morphology of compression fracture at the speeds of (a) 600 r/min, (b) 700 r/min, (c) 800 r/min, (d) 900 r/min

area, and the distribution of elements around the transition layer had significant changes when compared with that in Table 2. It can be seen that elements distribution is significantly different.

3.2 Mechanical Properties Test Results of the Composites

Based on the analysis results above, it can be seen that the microstructure and refinement degree of grains, as well as the size and distribution of carbides, are important factors in determining the hardness of the composite (Ref 27). The hardness of composites and eutectic carbide increased significantly with the centrifugal speed, as shown in Fig. 11(a). Figure 11(b) is the changed curve of Rockwell hardness from the radially inner surface to the outer surface of the composites at different centrifugal speeds. It can be seen that the Rockwell hardness of the composites reached its maximum at 900 r/min. This is in line with the previous conclusion about microstructure changes (Ref 31).

As seen in Fig. 12, the compressive strength of the composites increased with the centrifugal speed. At 900 r/min, the compressive strength was 1266 MPa. As the speed decreased to 600 r/min, the compressive strength was 1067 MPa. This was because, at 900 r/min the microstructure and carbide refinement of the composites were obvious, and its cutting effect on HCCI was smaller, thus their mechanical properties were improved under the synergistic effect of the matrix and carbides. From the morphology of compression fracture in Fig. 13, which changes with speeds, it can be seen that it had a brittle destructive fracture. At lower speeds, obviously the fracture was river pattern, with the fracture surface relatively smooth and flat, and it was mainly permeability fracture with coarse carbides. With the increase in centrifugal speed, the microstructure was refined and fine carbides were diffusely distributed, bringing better protection to the matrix, as a result of which the fracture started not from the

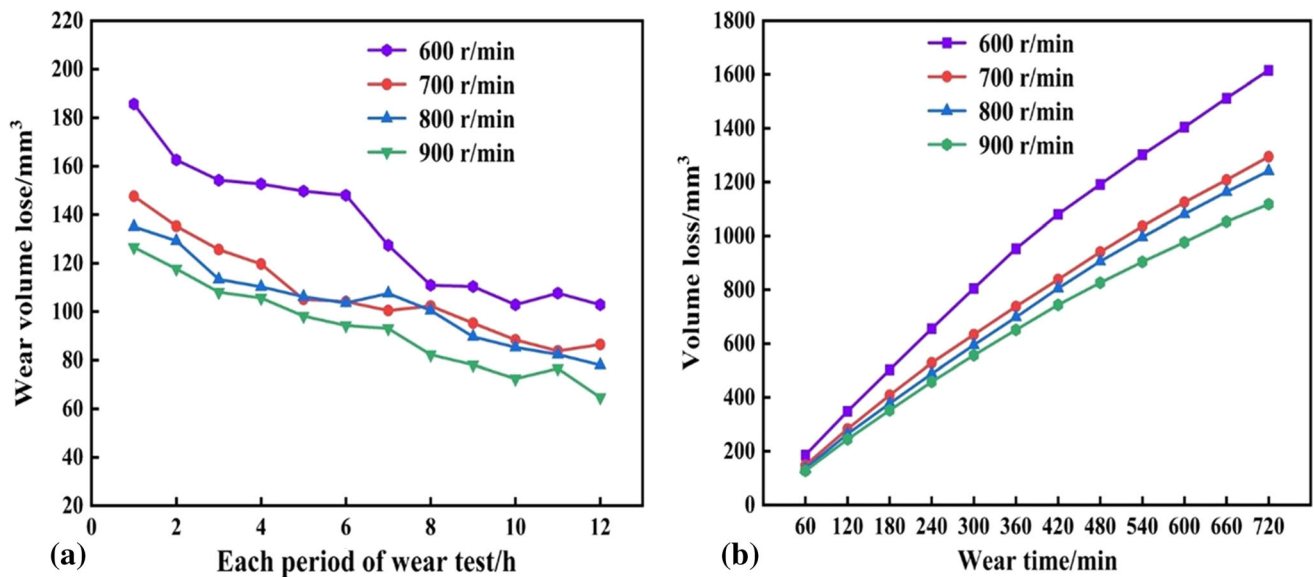


Fig. 14 (a) Relationship between the volume loss and periods of the wear tests at different speeds, (b) relationship between wear time and wear volume loss at different speeds

carbides but from junctions between the HCCI matrix and the ZTA ceramic particles. The compressive strength of the composites, therefore, rose with the centrifugal speed (Ref 32).

3.3 Three-Body Abrasion Wear Test results of the Composites

From Fig. 14, it can be seen that the volume wear loss of the composites decreased with the centrifugal speed, while the wear slowly decreased with wear time and tended to be stable. By comparison, the volume loss at 600 r/min was 1.45 times bigger than that at 900 r/min, so the wear resistance at 900 r/min was 1.45 times bigger than that at 600 r/min.

The wear morphology of the composites at different speeds was analyzed by using SEM, as shown in Fig. 15. At 600 r/min, there were pits as a result of spalling, deep plow grooves, and a few abrasives embedded in the HCCI matrix, and the ZTA particles were worn to a greater extent by rupture, accompanied by spalling in a small part of areas. When the speed was 900 r/min, the HCCI matrix looked flat with few pits and the ZTA particles were relatively intact, indicating that the hardness of the HCCI matrix became higher and the ZTA particles played a role in resisting wear at such a speed. However, the wear was severe near the area without ZTA particles, as shown in Fig. 15(c), and the step phenomenon was serious in these areas, which significantly highlighted the role of ZTA particles in promoting the wear resistance of the material. Thus with the increase in the centrifugal speed, the pits in the composites were found to gradually decrease, the plow grooves also decrease and become shallow, the ZTA particles fall off, and ruptures be reduced, which was because of the protection from the high-hardness HCCI matrix and ZTA particles, greatly reducing the wear loss of the composites. At the same time, it can be seen that the bond between ZTA particles and the HCCI matrix was still quite tight after the wear, and no cracks or defects were seen, which indicated that

the composites enjoy excellent bonding ability in their interface.

The schematic of the three-body abrasive wear mechanism of the ZTA/HCCI composites is shown in Fig. 16. At low centrifugal speeds, the HCCI matrix between ZTA particles had low hardness and poor wear resistance, and as the abrasive kept grinding and pressing back and forth under load, “grooves” were formed, which led to the lower support of the matrix, and some particles fell off to form pits, and the particles underwent severe wear. When the centrifugal speeds were high, the matrix had higher hardness and good wear resistance, producing stronger support and protection for ZTA particles, thus reducing significantly the wear of the composites. This is in line with the above microstructure analysis: the carbide microstructure at low centrifugal speeds was coarse, with poor fracture toughness and a strong cutting effect on the HCCI matrix. These abscission fragments acted as secondary abrasive, increasing wear rates during the wear process (Ref 33-35). This led to a decrease in the wear resistance of the composites (Ref 36, 37). At the same time, the larger size of austenite and its uneven distribution also contributed to the increase in wear. In contrast, when the centrifugal speed increased, austenite was refined and distributed continuously and uniformly, and fine carbides were diffusely distributed on the matrix, protecting it and reducing the areas undergoing wear. This is consistent with the results gained by Chang et. al (Ref 38).

In addition, during the wear process, the HCCI matrix with relatively low hardness was worn at the beginning, and later on the ZTA particles slowly protruded to become the main part receiving wear to protect the HCCI matrix from the abrasive particles cutting into it, which is called the “shadow protection effect.” Similarly, the HCCI matrix between the ZTA particles could provide good support for these particles, and both coordinated with each other to improve the wear resistance of the composites (Ref 39).

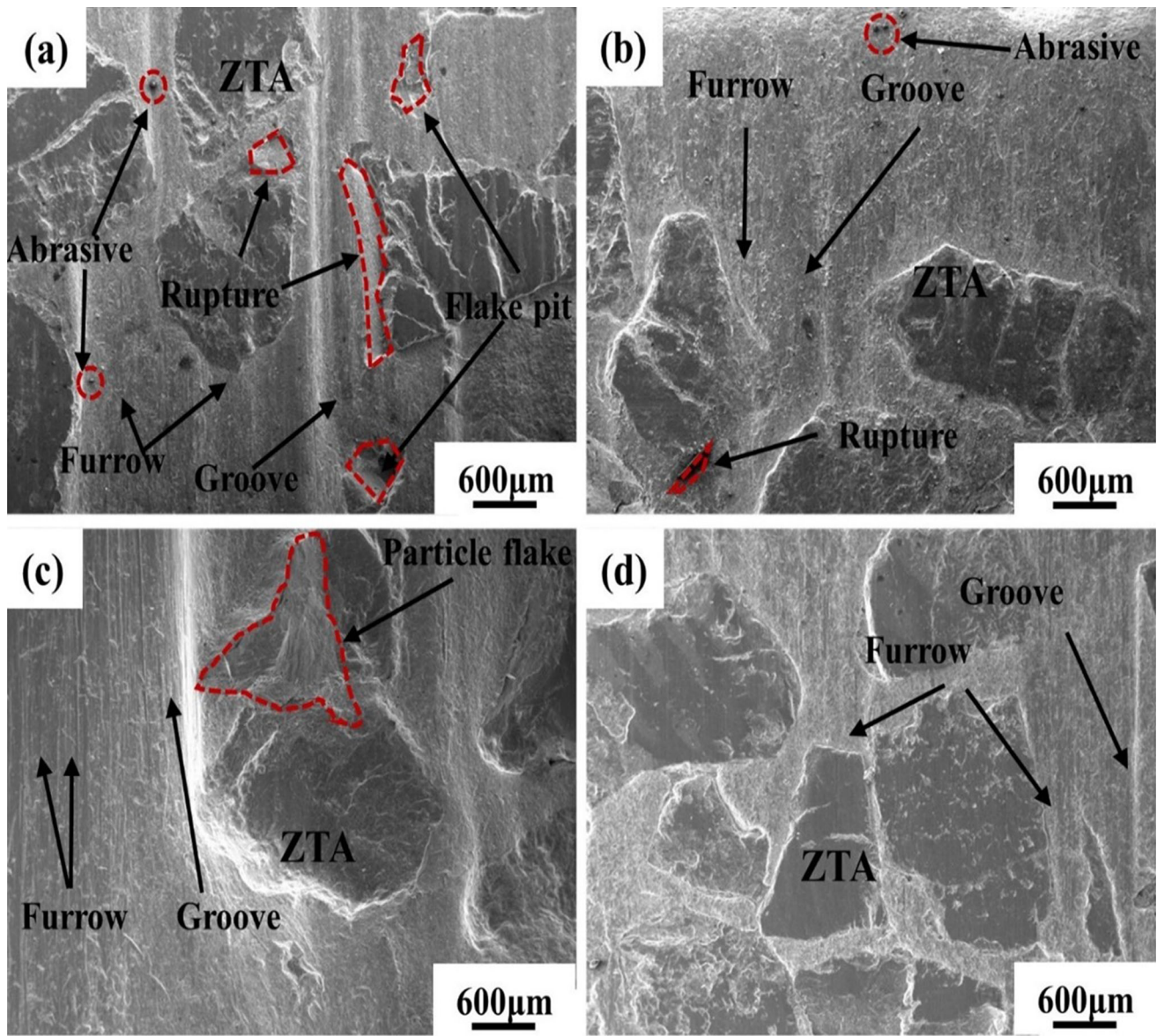


Fig. 15 The wear morphology of the sample at the speeds of (a) 600 r/min, (b) 700 r/min, (c) 800 r/min, (d) 900 r/min

4. Conclusions

In this study, the honeycomb-structured HCCI composites reinforced with ZTA particles were prepared by using centrifugal casting. Based on the investigation of the effect of speeds on the microstructure, mechanical properties, and wear resistance of the composites, the following conclusions can be drawn:

(1) The centrifugal speed is a very important parameter during the centrifugal casting process and has a significant effect on the microstructure of the composites. As the speed increased, the size of the primary austenite in the compos-

ites was reduced from 46 to 20 μm , the carbide size from 3.9 to 2.1 μm , and the volume fraction rose from 29.7 to 36.5%.

(2) As the centrifugal speed rose from 600 r/min to 900 r/min, the Rockwell hardness of ZTA/HCCI composites increased significantly, from 52 to 57 HRC, and their compressive strength increased from 1067 to 1266 MPa.

(3) As the speed increased, the composites experienced the least volume loss at the speed of 900 r/min, and their wear resistance at 900 r/min was 1.45 times bigger than at 600 r/min. The composite, therefore, enjoys the best wear resistance at 900 r/min.

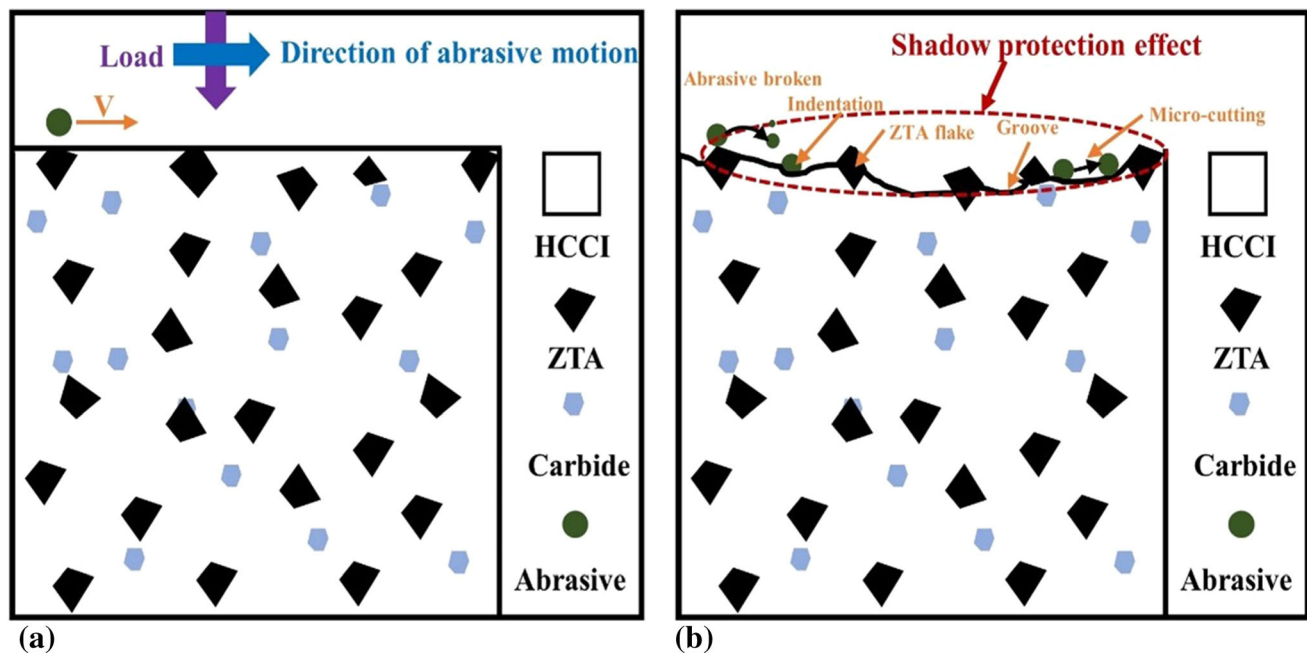


Fig. 16 Schematic of the wear failure mechanisms of ZTA/HCCI composites in the case of SiO₂ sands: (a) before wear, (b) after wear

Acknowledgments

This work was funded by the Yun Nan Fundamental Research Projects (grant NO.202101AU070155) and supported by the Talent Training Program of Kunming University of Science and Technology, China (KKS201901004).

Conflict of interest

The authors declare no conflict of interest.

References

- S.M. Zhao, X.M. Zhang, K.H. Zheng, J. Wang and L.I. Lin, Fabrication of ZTA/High Chromium Cast Iron Matrix Composites and Its Abrasive Wear Resistant [J], *Foundry Technol.*, 2011, **32**, p 1673–76
- Y.D. Sui, M.J. Zhou and Y.H. Jiang, Characterization Of Interfacial Layer of ZTA Ceramic Particles Reinforced Iron Matrix Composites, *J. Alloys Compd. Interdiscip. J. Mater. Sci. Solid-State Chem. Phys.*, 2018, **741**, p 1169–74.
- B. Jahani, M. Jazi Salimi, F. Azarmi and A. Croll, Effect of Volume Fraction Of Reinforcement Phase on Mechanical Behavior Of Ultra-High-Temperature Composite Consisting of Iron Matrix And TiB₂ particulates, *J. Compos. Mater.*, 2018, **52**, p 609–20.
- L. Zhong, F. Ye, Y. Xu, P. Yu, X.J. Liu, F.X. Ye and H.H. Yan, Microstructure And Abrasive Wear Characteristics of In Situ Vanadium Carbide Particulate-Reinforced Iron Matrix Composites [J], *Mater. Des.*, 2014, **54**, p 564–569.
- B. Qiu, S.M. Xing and Q. Dong, Fabrication and Wear Behavior of ZTA Particles Reinforced Iron Matrix Composite Produced by Flow Mixing and Pressure Compositing [J], *Wear*, 2019, **428**, p 167–177.
- H. Fu, Q. Xiao and J. Xing, Manufacture of Centrifugal Cast High Speed Steel Rolls for Wire Rod Mills [J], *Ironmak. Steelmak.*, 2004, **31**, p 389–392.
- W. Huisman, T. Graule and L.J. Gauckler, Alumina of High Reliability by Centrifugal Casting [J], *J Eur. Ceram. Soc.*, 1995, **15**, p 811–821.
- B. Saleh, J. Jiang, A. Ma, G. Song and D.H. Yang, Effect of Main Parameters on the Mechanical and Wear Behaviour of Functionally Graded Materials by Centrifugal Casting: A Review [J], *Met. Mater. Int.*, 2019, **25**, p 1395–1409.
- S. Jamaludin, F. Mustapha, D.M. Nuruzzaman and S.N. Basri, A Review on the Fabrication Techniques of Functionally Graded Ceramic-Metallic Materials in Advanced Composites [J], *Sci. Res. Essays*, 2013, **8**, p 828–840.
- N. Radhika and R. Raghu, Development of Functionally Graded Aluminium Composites using Centrifugal Casting and Influence of Reinforcements on Mechanical and Wear Properties [J], *Trans. Nonferrous Met. Soc. China*, 2016, **26**, p 905–916
- Y.P. Song and H.G. Wang, The Microstructure and Properties of Restored WCP/Fe-C Composites [J], *Adv. Mater. Res.*, 2011, **194**, p 2105–2108
- C. Yang, Y.Q. Chun, J.P. Xu, H.M. Yang and L. Peng, Study on Technology and Process of Centrifugal Micro Casting Based on Permanent Mold [J], *J. Heilongjiang Inst. Technol.*, 2014, **28**, p 48–51
- L. Niu, M. Hojamberdiev and Y. Xu, Preparation of In Situ-Formed Wc/Fe Composite on Gray Cast Iron Substrate by A Centrifugal Casting Process [J], *J. Mater. Process. Technol.*, 2010, **210**, p 1986–1990.
- E. Panda, S.P. Mehrotra and D. Mazumdar, Mathematical Modeling of Particle Segregation during Centrifugal Casting of Metal Matrix Composites [J], *J. Mater. Eng. Perform.*, 2012, **21**, p 450–462.
- H. Shimazaki, R. Miyawaki, K. Yokoyama and S. Matsubara, A Reconnaissance Study on Minerals from the Bayan Obo Nb-REE-Fe Deposit, Inner Mongolia, China [J], *Bull. Natl. Sci. Mus. Tokyo Ser. C*, 2008, **34**, p 1–26
- F.U. Hanguang, X.I.A.O. Qing and X.I.N.G. Jiandong, A Study of Segregation Mechanism in Centrifugal Cast High Speed Steel Rolls [J], *Mater. Sci. Eng. A*, 2008, **479**, p 253–260.
- J. Honda, Trana, *ISIJ*, 1984, **24**, p 85–100.
- K. Zheng, Y. Gao, S. Tang, Y. Li, S. Ma, D. Yi and Z. Zhang, Interface Structure and Wear Behavior of Cr26 Ferrous Matrix Surface Composites Reinforced with CTCP [J], *Tribol. Lett.*, 2014, **54**, p 15–23.
- Y. Li and Y. Gao, Three-Body Abrasive Wear Behavior of CC/high-Cr WC Composite and Its Interfacial Characteristics [J], *Wear*, 2009, **268**, p 511–518.
- B. Qiu, S. Xing, Q. Dong and H. Liu, Comparison of Properties and Impact Abrasive Wear Performance of ZrO₂-Al₂O₃/Fe Composite Prepared by Pressure Casting and Infiltration Casting Process, *Tribol. Int.*, 2020, **142**, p 105979.
- Y.W. Sui, B.S. Li, A.H. Liu, J. Guo and J. Fu, Z H, J, Evolution of Solidification Microstructure of Centrifugal Cast Ti–6Al–4V Alloy [J], *Met. Sci. J.*, 2013, **25**, p 1458–1461.
- Emmott J G. INTRODUCTION, [J]. *Appl. Sci. Cast. Met.*, 1970p vii–viii

23. A. Halvae and A. Talebi, Effect of Process Variables on Microstructure and Segregation In Centrifugal Casting of C92200 Alloy [J], *J. Mater. Process. Technol.*, 2001, **118**, p 122–126.
24. J. Zhang, Z. Fan, Y. Wang and B. Zhou, Hypereutectic Aluminium Alloy Tubes with Graded Distribution of Mg₂Si Particles Prepared by Centrifugal Casting [J], *Mater. Des.*, 2000, **21**, p 149–153.
25. B. Dutta and M.K. Surappa, Microstructure Evolution during Multidirectional Solidification of Al-Cu-SiC Composites [J], *Compos. A Appl. Sci. Manuf.*, 1998, **29**, p 565–573.
26. Ö. Doğan, J. Hawk and G. Laird, Solidification Structure and Abrasion Resistance of High Chromium White Irons [J], *Metall. Mater. Trans. A.*, 1997, **28**, p 1315–1328.
27. Y. Luan, N. Song, Y. Bai, X. Kang and D. Li, Effect of Solidification Rate on the Morphology and Distribution of Eutectic Carbides in Centrifugal Casting High-Speed Steel Rolls [J], *J. Mater. Process. Technol.*, 2010, **210**, p 536–541.
28. A. Ac, A. Smc, A. Mj and B. Lb, Austenite Grain Growth and Hot Deformation Behavior in A Medium Carbon Low Alloy Steel [J], *J. Market. Res.*, 2020, **9**, p 12102–12114.
29. H. Quyen, V.A. Tuan, T.P. Dong, V.V. Quyen and N.D. Nam, Effect of Rare Earth on M7C3 Eutectic Carbide in 13% Chromium Alloy Cast Iron [J], *Int. J. Adv. Sci. Eng. Inf. Technol.*, 2019, **9**, p 724.
30. P. Li, X. Li, Y. Li, M. Gong and W. Tong, Microstructure and Mechanical Properties of Millimeter WC Particle-Reinforced High-Chromium Cast Iron Composites [J], *J. Mater. Eng. Perform.*, 2019, **28**, p 7816–7827.
31. G. Niu, Y. Sui, H. Zeng, Y. Jiang and M. Zhou, Effect of Centrifugal Casting Temperature on the Microstructure and Properties of ZTAP/HCCI Matrix Composites [J], *Mater. Res. Exp.*, 2021, **8**, p 026513.
32. C. Wang, M. Wang, S. Jie, W. Hui and D. Han, Effect of Microstructure Refinement on the Strength and Toughness of Low Alloy Martensitic Steel [J], *J. Mater. Sci. Technol.*, 2007, **23**, p 659–664.
33. Y. Jian, Z. Huang, J. Xing and J. Li, Effects of Chromium Additions on the Three-Body Abrasive Wear Behavior of Fe-3.0 wt% B alloy, *Wear*, 2017, **378–379**, p 165–173.
34. X.H. Tang, R. Chung, C.J. Pang, D.Y. Li, B. Hinckley and K. Dolman, Microstructure of High (45wt.%) Chromium Cast Irons and Their Resistances to Wear and Corrosion, *Wear*, 2011, **271(9–10)**, p 1426–1431. <https://doi.org/10.1016/j.wear.2010.11.047>
35. E. Guo, L. Wang, L. Wang and Y. Huang, Effects of RE, V, Ti and B Composite Modification on the Microstructure and Properties of High Chromium Cast Iron Containing 3% Molybdenum [J], *Chin. J. Rare Met.*, 2009, **28**, p 6.
36. K.H. Zheng, Y.M. Gao, Y. Li, S.M. Zhao and J. Wang, Three-Body Abrasive Wear Resistance of Iron Matrix Composites Reinforced with Ceramic Particles [J], *Proc. Inst. Mech. Eng. Part –J. Eng. Tribol.*, 2013, **228**, p 3–10.
37. M.J. Zhou, Y.D. Sui, X.Y. Chong and Y.H. Jiang, Wear Resistance Mechanism of ZTAP/HCCI Composites with a Honeycomb Structure [J], *Met. - Open Access Metall. J.*, 2018, **8**, p 588.
38. K.K. Chang, S. Lee, J.Y. Jung and S. Anh, Effects of Complex Carbide Fraction on High-Temperature Wear Properties of Hardfacing Alloys Reinforced with Complex Carbides [J], *Mater. Sci. Eng., A*, 2003, **349**, p 1–11.
39. Z.L. Li, Y.H. Jiang and Z. Rong, Dry Three-Body Abrasive Wear Behavior of WC Reinforced Iron Matrix Surface Composites Produced by V-EPC Infiltration Casting Process [J], *Wear*, 2007, **262**, p 649–654.

Publisher's Note Springer Nature remains neutral with regard to jurisdictional claims in published maps and institutional affiliations.